

Photospheric Emission of Gamma-Ray Bursts

A. M. Beloborodov · P. Mészáros

Received: date / Accepted: date

Abstract We review the physics of GRB production by relativistic jets that start highly opaque near the central source and then expand to transparency. We discuss dissipative and radiative processes in the jet and how radiative transfer shapes the observed nonthermal spectrum released at the photosphere. A comparison of recent detailed models with observations gives estimates for important parameters of GRB jets, such as the Lorentz factor and magnetization. We also discuss predictions for GRB polarization and neutrino emission.

Keywords Gamma-Ray Bursts · Radiative processes

1 Introduction

The emission mechanism of gamma-ray bursts (GRBs) has been a puzzle since their discovery half a century ago. Following the discovery of GRB afterglows in the end of 1990s, it has been established that GRB emission arises in ultra-relativistic jets from extremely powerful cosmic explosions at cosmological distances. The existing emission models are mainly guided by the observed spectrum of the jet radiation and its fast variability.

The main phase of a GRB, usually called “prompt” emission, typically lasts seconds or minutes, with huge luminosities, sometimes reaching $L_\gamma \sim 10^{54}$ erg s⁻¹ in isotropic equivalent (before correcting for the beaming of radiation from a collimated relativistic jet). The prompt phase should be dis-

A. M. Beloborodov
Physics Department and Columbia Astrophysics Laboratory, Columbia University, 538 West
120th Street, New York, NY 10027, USA
E-mail: amb@phys.columbia.edu

P. Mészáros
Center for Particle and Gravitational Astrophysics, Dept. of Astronomy & Astrophysics and
Dept. of Physics, Pennsylvania State University, University Park, PA 16802, USA
E-mail: nnp@psu.edu

tinguished from the GRB “afterglow” — the long-lasting and weaker emission with a broad spectrum extending from gamma-rays to radio waves.

The spectrum of prompt emission has a well defined, sharp peak at an energy E_{pk} that varies around 1 MeV, after correcting by $1+z$ for the cosmological redshift (Kaneko et al. 2006; Goldstein et al. 2012). For most bursts the spectrum around the peak can be approximately described by a simple Band function (Band et al. 2009) — two power laws that are smoothly connected at E_{pk} . Bursts of higher luminosity are observed to have higher E_{pk} . An approximate correlation $E_{\text{pk}} \approx 0.3 L_{\gamma,52}^{1/2}$ MeV was reported (e.g. Wei and Gao (2003); Yonetoku et al. (2004); Ghirlanda et al. (2012)), where $L_{\gamma,52}$ is the burst luminosity (isotropic equivalent) in units of 10^{52} erg s $^{-1}$.

The short durations of $\sim 0.1 - 10$ s and fast variability of GRB emission imply that it is produced by outflows or jets with Lorentz factors $\Gamma \gtrsim 10^2$. The Doppler effect compresses the typical observed timescale of radiation released at a radius r , from $\sim r/c$ to $\sim r/c\Gamma^2$. In addition, a high Γ allows the radiation to decouple from the jet at smaller radii; typically, the jet becomes transparent to MeV radiation at radii somewhere between 10^{12} and 10^{14} cm. The characteristic scattering optical depth seen by photons propagating from a radius r to infinity is given by

$$\tau_{\text{T}} = \frac{Z_{\pm} \dot{M}_p \sigma_{\text{T}}}{4\pi r \Gamma^2 m_p c}, \quad (1)$$

where \dot{M}_p is the isotropic equivalent of the proton mass outflow rate, and Z_{\pm} is the number of e^{\pm} per proton. The optically thin zone of the jet roughly corresponds to $\tau_{\text{T}} < 1$, and the sub-photospheric region is where $\tau_{\text{T}} > 1$. Strong energy dissipation must occur in the jet to generate the observed non-thermal spectra. This dissipation can occur before and after the jet becomes transparent to radiation.

1.1 Optically thin synchrotron emission?

A simple phenomenological GRB model posits that we observe Doppler-shifted synchrotron radiation, similar to blazar jets. The model assumes that a non-thermal electron population is injected in the jet by some dissipative process in an optically thin outflow. It gives a radiation spectrum that peaks at the photon energy

$$E_{\text{pk}} \approx E_{\text{syn}} = 0.4 \Gamma \gamma_{\text{pk}}^2 \hbar \frac{eB}{m_e c}. \quad (2)$$

Here B is the magnetic field measured in the rest frame of the jet (“fluid frame”), γ_{pk} is the Lorentz factor at which the injected electron distribution peaks (also measured in the fluid frame), and Γ is the bulk Lorentz factor of the jet itself. If the electron distribution at $\gamma_e > \gamma_{\text{pk}}$ is a power-law $dN_e/d\gamma_e \propto \gamma_e^{-p}$ then the synchrotron spectrum has a high-energy power-law tail, $dN_{\text{ph}}/dE \propto E^{-p/2-1}$ at $E > E_{\text{pk}}$.

One possibility for the injection of high-energy electrons is associated with internal shocks (Rees and Mészáros 1994; Kobayashi et al. 1997; Daigne and Mochkovitch 1998). A mildly relativistic electron-ion shock produces an electron distribution with $\gamma_{\text{pk}} \sim \epsilon_e (m_p/m_e)$, where ϵ_e can be a significant fraction of unity. This gives

$$E_{\text{pk}} \approx 1 r_{12}^{-1} \epsilon_B^{1/2} L_{52}^{1/2} \left(\frac{\epsilon_e}{0.3} \right)^2 \text{ MeV}, \quad (3)$$

where r_{12} is radius in units in 10^{12} cm, L_{52} is the isotropic equivalent of the jet power in units of 10^{52} erg s^{-1} , and ϵ_B is the fraction of jet energy that is carried by the magnetic field. If the shock radius happens to be $r \sim 10^{13} \epsilon_B^{1/2} \epsilon_e^2$ cm then E_{pk} would be consistent with observations. A Band-type spectrum is emitted if the electron energy distribution extends as a power law at $\gamma_e > \gamma_{\text{pk}}$ and cuts off at $\gamma_e < \gamma_{\text{pk}}$, with a negligible Maxwellian component (e.g. Burgess et al. (2011)). This is a problematic requirement. In observed shocks, e.g. in the solar system or in supernovae, as well as in computer-simulated shocks, most of the dissipated energy is given to Maxwellian particles, with only a small fraction of particles populating the high-energy nonthermal tail.

Strong magnetization $\epsilon_B \gtrsim 0.1$ offers an alternative mechanism for particle acceleration: the dissipation of magnetic energy, in particular through magnetic reconnection (Drenkhahn and Spruit 2002). Recent dedicated numerical studies of relativistic reconnection show that it gives a broad flat electron distribution, with no cutoff at low energies (Kagan et al. 2015). Synchrotron emission from this electron distribution does not resemble the pronounced spectral peak observed in GRBs.

The synchrotron model may be viewed more broadly as a phenomenological model which does not specify how the desired electron distribution is created. In this form the model still faces a few problems:

- (1) Thousands of GRBs have been observed, and most of them have E_{pk} near 1 MeV (Goldstein et al. 2012). Few bursts have E_{pk} above 10 MeV and no bursts are known with $E_{\text{pk}} > 20$ MeV. This is at odds with the naive model prediction $E_{\text{pk}} \propto \Gamma \gamma_{\text{pk}}^2 B$, which should give a broad distribution of E_{pk} due to variations in the local B , γ_{pk} , and Γ .
- (2) High-energy electrons quickly cool to $\gamma_e < \gamma_{\text{pk}}$ (which makes the process radiatively efficient) and should emit radiation at $E < E_{\text{pk}}$ with a photon index $\alpha = -3/2$. A typical low-energy index observed in GRBs is $\alpha \sim -1$, and many bursts have even harder slopes $\alpha > 0$ (Kaneko et al. 2006). Such hard slopes are in conflict with the synchrotron model.
- (3) The synchrotron spectrum should have a rather broad peak, even when the source is assumed to have a uniform magnetic field B and the power-law electron distribution is assumed to cut off at $\gamma_e < \gamma_{\text{pk}}$. Attempts to reproduce GRB spectra with such idealized models gave acceptable fits for a small number of bursts (Burgess et al. 2011, 2014; Preece and the Fermi collab. 2014) and were found incompatible with observed spectra in the dominant majority of GRBs (Axelsson and Borgonovo 2015; Yu et al. 2015).

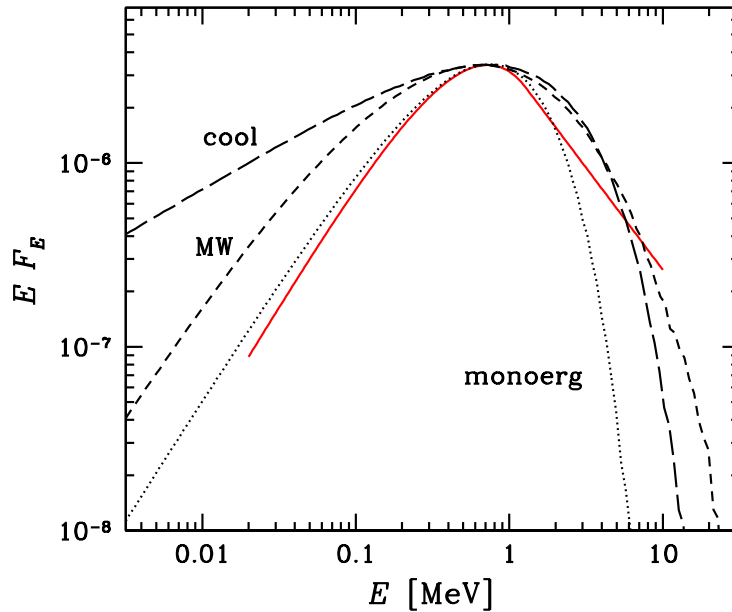


Fig. 1 Synchrotron spectra from an optically thin spherical shell. Three models are shown with different electron distributions: mono-energetic (dotted line), Maxwellian (short-dashed line), and fast-cooling Maxwellian (long-dashed line). For comparison the Band fit of GRB 990123 is shown by the red curve. (From Vurm and Beloborodov (2016b).)

The peak sharpness problem is illustrated in Figure 1 where a synchrotron spectrum is compared with the Band fit of a bright burst with a typical spectrum, GRB 990123. In the realistic fast-cooling regime, the minimum width of the synchrotron peak at half maximum exceeds 1.5 orders in photon energy, even with a single value of B in the emitting source and the narrow injected electron distribution (single-temperature Maxwellian). It is significantly broader than the Band fit to the *time-average* of the GRB spectrum (Briggs et al. 1999). Uncertainties in the observed spectrum due to the detector response and limited photon statistics allow some room for stretching the measured peak width; however it can hardly be made consistent with the synchrotron model, especially when the inevitable broadening due to variable magnetic fields, electron injection and the Doppler factor are taken into account. Note also that synchrotron spectra with sharp peaks consistent with a Band function are not observed in any other astrophysical objects. One example is provided by blazars — their synchrotron spectra have the half-maximum width of several orders of magnitude, broader than in GRBs (e.g. Ghisellini (2006)).

1.2 Photospheric emission

The sharp MeV spectral peak provides evidence for thermalization of radiation at early, opaque stages of the GRB explosion (Paczýnski (1986); Goodman (1986); Thompson (1994); Mészáros and Rees (2000b)). The inheritance of the spectral peak from an initial thermalization stage is also supported by the observed distribution of E_{pk} , which cuts off above ~ 10 MeV in agreement with a theoretical maximum (Beloborodov 2013).

Accepting that the MeV peak forms inside an opaque jet leads to so-called “photospheric” emission models: the GRB radiation is released where the jet becomes transparent to scattering. Several versions of the photospheric model have been discussed over the years (Thompson 1994; Eichler and Levinson 2000; Rees and Mészáros 2005; Giannios and Spruit 2007; Beloborodov 2010; Levinson 2012; Thompson and Gill 2014). All share a key feature: the jet is *dissipative*, i.e. significantly heated as it propagates away from the central engine. This heating modifies the emitted photospheric radiation from simple blackbody emission. The resulting spectrum was investigated using dedicated numerical simulations and found to have a nonthermal shape that closely resembles the phenomenological Band function (Pe’er et al. (2006); Giannios (2008); Beloborodov (2010); Vurm et al. (2011); Gill and Thompson (2014); Vurm and Beloborodov (2016b)). It was proposed that the dissipative photosphere provides the best description for the observed spectra (e.g. Ryde et al. 2011).

Previous observational search for photospheric emission mainly looked for a Planck component or its modifications, see Pe’er (2016) for a recent review. In contrast, the detailed theoretical calculations suggest that photospheric emission has a broad Band-like spectrum that dominates the prompt GRB rather than adds a blackbody component to it.

2 Sub-photospheric dissipation

Internal bulk motions and magnetic fields provide energy reservoirs available for dissipation in GRB jets. Three mechanisms can make photospheric emission nonthermal:

1. Dissipation of magnetic energy
2. Collisions of drifting neutrons
3. Internal shocks

The details of magnetic dissipation are complicated and still poorly understood. The other two dissipation mechanisms can be examined from first principles and give predictions that can be compared with observations; we will discuss them in some detail below.

A neutron component is expected in GRB explosions (Derishev et al. 1999; Bahcall and Mészáros 2000; Mészáros and Rees 2000a; Beloborodov 2003; Rossi et al. 2006). Free neutrons enter the jet from the neutronized central

engine and are also produced by spallation reactions in the jet itself. They begin to drift with respect to the proton flow in the sub-photospheric region and collide with the protons. These nuclear collisions create pions, whose decay leads to the production of e^\pm pairs with Lorentz factors $\gamma_e \sim m_\pi/m_e \sim 300$ in the jet rest frame and to the emission of neutrinos with energy $\sim \Gamma m_\pi c^2$ in the observer frame. These multi-GeV neutrinos are detectable with IceCube (Bartos et al. 2013; Murase et al. 2013) and can provide an important test for GRB models. The photospheric spectrum generated by neutron collisions has been calculated by Beloborodov (2010) and Vurm et al. (2011), and found to be consistent with GRB spectra.

Internal shocks are generally expected to develop in GRB jets, as the jets are highly variable. The central engine of the explosion is likely unsteady, and additional variability is induced as the jet breaks out of the progenitor star (Lazzati et al. 2009, 2013; Ito et al. 2015). This breakout is accompanied by multiple internal and recollimation shocks. Shock heating is expected to occur in an extended range of radii and in an extended range of timescales, which is consistent with the broad power spectrum of variability observed in GRB light curves (Beloborodov et al. 2000; Morsony et al. 2010).

As long as the flow is opaque and radiation dominates its energy density, photon diffusion plays a leading role in shaping the shock front. Its thickness is then comparable to the photon mean free path. The radiation-mediated shock (RMS) is not capable of electron acceleration by the standard Fermi mechanism, since the electron radiates its energy much faster than it can cross the shock. Photons can experience significant energy gains by crossing the shock back and forth multiple times (Blandford and Payne 1981; Riffert 1988; Levinson 2012). This “bulk Comptonization” upscatters photons up to the MeV band (in the fluid frame). Upscattering to higher energies is hindered by the energy loss due to electron recoil in scattering. Photon upscattering beyond ~ 1 MeV is also stopped by the absorption reaction $\gamma + \gamma \rightarrow e^- + e^+$, and the produced mildly relativistic e^\pm pairs quickly cool down due to Coulomb and inverse Compton (IC) losses.

All this would suggest that sub-photospheric shocks are inefficient in producing particles with energies $E \gg m_e c^2$ in the fluid frame. However, a more realistic picture of sub-photospheric shocks differs from the simple RMS, in particular in outflows that carry magnetic fields and free neutrons in addition to the plasma and radiation. The shock wave is capable of generating ultra-relativistic electrons in two ways:

- A strong collisionless subshock forms in the RMS. This is inevitable (even deep below the photosphere) if the flow is sufficiently magnetized (Beloborodov 2016). A mildly relativistic collisionless subshock heats the electrons to an ultra-relativistic temperature T_e , as they receive a significant fraction of the ion kinetic energy (e.g. Sironi and Spitkovsky 2011). One can show that the inverse Compton (IC) emission from the heated electrons breeds e^\pm pairs in the upstream, and this process regulates the subshock temperature to $kT_e \sim 10m_e c^2$.

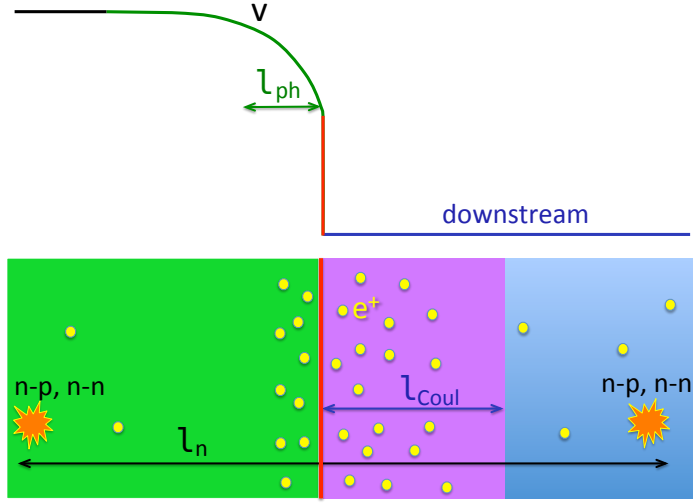


Fig. 2 Structure of a relativistic internal shock in a hot, opaque, magnetized outflow. The green part of the velocity profile is shaped by radiation pressure on a scale comparable to the photon mean free path to scattering, l_{ph} . The vertical red part is the collisionless subshock, which heats ions to a mildly relativistic temperature and electrons to an ultra-relativistic temperature. The ultra-relativistic electrons are quickly cooled, producing synchrotron and inverse Compton (IC) photons, which create e^{\pm} pairs ahead and behind the shock. The ion cooling occurs on a longer scale l_{Coul} , which exceeds the RMS thickness if the subshock is relativistic. In the presence of a free neutron component in the flow, the shock wave is partially shaped by neutron migration between the upstream and downstream. The neutron mean free path ℓ_n is the longest scale in the shock structure. The migrating neutrons are stopped by nuclear collisions. Inelastic nuclear collisions result in injection of e^{\pm} with Lorentz factors $\gamma_e \sim m_{\pi}/m_e \sim 300$, distributed over a broad region $\sim \ell_n$. The nuclear collisions also emit neutrinos; they escape the outflow with energies $\sim \Gamma m_{\pi} c^2$ where Γ is the outflow Lorentz factor. (From Beloborodov (2016).)

- Inelastic nuclear collisions inject e^{\pm} pairs with Lorentz factors $\sim m_{\pi}/m_e \sim 300$ in the fluid frame. This mechanism becomes particularly efficient if the outflow carries free neutrons, as they can migrate across the RMS, making the shock wave partially mediated by neutrons (Figure 2).

The structure of sub-photospheric shocks can be studied using detailed numerical simulations. One method is to search for a steady-state propagating solution of the kinetic equations (e.g. Levinson and Bromberg (2008); Budnik et al. (2010)), which may be found by iterations. Alternatively, one can use direct time-dependent simulations of shock formation. The simulation can be set up to follow the evolution of a compressive wave in the outflow, which leads to formation of a pair of shocks and their subsequent quasi-steady propagation. Then the shock structure is obtained from first principles by calculating the time-dependent radiative transfer through the moving plasma. A detailed first-

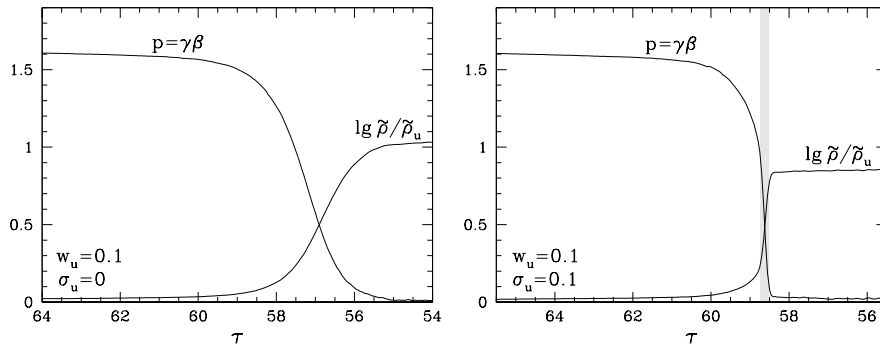


Fig. 3 Snapshot of a shock propagating in the flow with upstream radiation enthalpy $w_u = 0.1$ and upstream magnetization $\sigma_u = 0$ (left) and 0.1 (right). The parameters w and σ are defined in the fluid frame as $w = (4/3)U_{\text{rad}}/\tilde{\rho}c^2$ and $\sigma = B^2/4\pi\tilde{\rho}c^2 = 2\varepsilon_B$, where U_{rad} is the radiation energy density and $\tilde{\rho}$ is the proper mass density of the fluid. The shock is propagating to the left and the Thomson optical depth τ is measured from the site of shock formation (caustic of the initial supersonic wave). The solid curves show the profiles of momentum $p = \gamma\beta$ and proper density $\tilde{\rho}$ (normalized to the upstream proper density $\tilde{\rho}_u$). A strong subshock has formed in the magnetized case; it is highlighted by the grey strip. The electron temperature has a strong and narrow peak at the subshock. The subshock is resolved (not a discontinuous jump) due to a finite viscosity employed in the simulation of the plasma dynamics. The radiation is everywhere simulated directly as a large collection of individual photons whose propagation and scattering is followed using the Monte-Carlo technique. (From Beloborodov (2016).)

principle simulation involves tracking of a large number of individual photons and their interaction with the moving plasma (using Monte-Carlo techniques).

The shock structure obtained with this method is shown in Figure 3, for two cases — with and without magnetic fields. The simulations demonstrate the formation of a strong collisionless subshock in the magnetized RMS. In GRB jets, a moderate magnetization ~ 0.1 is sufficient to generate a strong subshock.

Electron-positron pair creation was expected in dissipative GRB jets since the early works in the 1990s (e.g. Rees and Mészáros (1994); Thompson (1994); Mészáros and Rees (2000b)). The efficiency of this process is described by the pair loading factor $Z_{\pm} = n_{\pm}/n_p$ where n_p is the proton density and n_{\pm} is the e^{\pm} density. One can show that Z_{\pm} reaches a peak of $\sim 10^2$ inside the shock front and decreases behind it due to pair annihilation (Beloborodov 2016). The pairs are produced in collisions between MeV photons, which are generated by two mechanisms: (1) An RMS without a strong collisionless subshock produces MeV photons due to bulk Comptonization by a relatively cold flow (the flow is everywhere in local Compton equilibrium with radiation at $kT \ll m_e c^2$). (2) In the presence of a collisionless jump, MeV photons are produced by IC cooling of e^{\pm} heated to the subshock temperature $kT_e \sim 10m_e c^2$.

The shock “breakout” at the photosphere¹ occurs through the growth of the collisionless jump in the RMS until radiation completely decouples from the plasma. Eventually the entire velocity jump becomes mediated by collective plasma processes, regardless of magnetization. This somewhat resembles the shock breakout in non-relativistic supernova explosions (Waxman and Loeb 2001; Giacinti and Bell 2015). However, the photospheric shock breakout in GRBs has a special feature: e^\pm pair creation. The shock sustains a local optical depth $\tau_T \gtrsim 1$ even after the background electron-ion plasma becomes transparent. Effectively, the shock carries the photosphere with it until it expands by an additional factor $\sim 30 - 100$, continually producing photospheric emission (Beloborodov 2016). This emission should be observed as a prominent pulse of nonthermal radiation in the GRB light curve. In the observer frame, the emission from the e^\pm -dressed shocks extends up to the GeV band, where γ - γ absorption shapes a break in the spectrum.

The high-energy photospheric pulses contribute to the prompt GRB emission. This emission is observed to overlap (in arrival time) with GeV afterglow, which is associated with the external blast wave from the explosion (Ackermann and The Fermi collaboration 2013). The early peak of GeV afterglow is explained by the e^\pm -loading of the blast wave (Beloborodov et al. 2014; Hascoët et al. 2015), and its overlap with the high-energy photospheric pulses can explain the observed variable component of GeV emission at early times.

Internal shocks are the main heating mechanism for jets that are not dominated by magnetic fields. This is a likely situation in GRBs, as comparison of detailed models of photospheric radiation with observed GRB spectra suggests a moderate magnetization in the sub-photospheric region, $\sigma \sim 10^{-2} - 10^{-1}$ (see Section 4 below). This does not exclude a stronger magnetization closer to the central engine, allowing for magnetic dissipation that reduces σ as the jet expands. In this scenario, the early heating at very large optical depths may be dominated by magnetic dissipation. Constraints on the jet magnetization at small radii were recently estimated using the jet breakout time by Bromberg et al. (2015); they find that the jet is not dominated by magnetic fields.

Neutron migration across the shock front leads to nuclear collisions which generate additional e^\pm pairs and produce neutrino emission. The typical observed energy of neutrinos produced by this mechanism is $\sim \Gamma m_\pi c^2 \gtrsim 10$ GeV. Sub-photospheric internal shocks were also proposed to emit ultra-high-energy neutrinos (Mészáros and Waxman 2001; Razzaque et al. 2003). This proposal assumes efficient ion acceleration by the Fermi diffusive mechanism, which does not operate in an RMS and requires a collisionless (sub)shock. Diffusive acceleration is, however, suppressed in shocks with a transverse magnetic field, which advects the particles downstream before they have a chance to cross the shock many times (Sironi and Spitkovsky 2011). Obliqueness of the magnetic field could help the ion acceleration. Another possible way to accelerate ions is the converter mechanism proposed by Derishev et al. (2003). Numerical

¹ The photospheric shock breakout should not be confused with the jet breakout from the progenitor star. The jet breakout occurs at smaller radii and huge optical depths.

simulations of Kashiyama et al. (2013) suggest that the converter mechanism becomes efficient for ultra-relativistic shocks, with amplitude $\gamma_0 \gtrsim 4$. This mechanism is, however, quite slow as it relies on neutron-to-proton and proton-to-neutron conversion in (inelastic) nuclear collisions, which occur with a large free path $l_n \sim (n_p \sigma_n)^{-1}$ due to the modest nuclear cross section $\sigma_n \approx \sigma_T/20$.

3 Peak position of the photospheric spectrum E_{pk}

Photons deep below the photosphere keep interacting with the plasma, and their spectrum forms a sharp Wien peak. The simplest model of photospheric emission assumes a freely expanding radiation-dominated outflow with no baryon loading or magnetic fields (Paczýnski 1986; Goodman 1986). In this case, dissipation weakly influences the radiation spectrum and it is not far from a Planck shape. The peak energy of the Planck spectrum (defined as the peak of $dL/d\ln E$) is related to the average photon energy \bar{E} by $E_{\text{pk}} \approx 1.45\bar{E}$. In the ideal radiation-dominated outflow \bar{E} remains constant and equal to its value near the central engine E_0 .

This simple dissipationless model, however, fails to explain the observed spectra. Although the Planck spectrum may appear in the time-resolved emission of some bursts (e.g. Ryde (2004); Ryde et al. (2011)), GRB spectra are typically nonthermal, with an extended high-energy tail.

3.1 Effects of collimation and early dissipation

The average photon energy at the explosion centre, E_0 , is a useful parameter of more general jets, which may be dissipative, magnetized, and collimated. E_0 may be expressed in terms of the jet power L_0 and an initial radius r_0 (comparable to the size of the central compact object) using the relation $\epsilon_0 L_0 \approx 4\pi r_0^2 a T_0^4 c$,

$$E_0 \approx 10 \epsilon_0^{1/4} L_{0,52}^{1/4} r_{0,6}^{-1/2} \text{ MeV}. \quad (4)$$

Here ϵ_0 is the initial thermal fraction of the power L_0 (radiation-dominated jets with sub-dominant magnetic energy have $\epsilon_0 \approx 1$). Collimation of the flow within a small angle θ_c implies a smaller true jet power L_0 compared with its apparent isotropic equivalent L_γ ,

$$L_0 \approx \frac{\theta_c^2}{2} L_\gamma, \quad (5)$$

and hence E_0 is reduced as $\theta_c^{1/2}$. Achromatic breaks in GRB afterglow light curves are often interpreted as evidence for jet collimation, with a typical opening angle of 5-10°. Collimation helps explain the extremely high apparent luminosities L_γ , which reach 10^{54} erg s⁻¹ in some GRBs. This collimation can be the result of the pressure confinement of the jet by the progenitor star and the breakout cocoon, or by a dense wind from the outer regions of the

central accretion disk. Collimation may also be assisted by strong magnetic fields (Komissarov et al. 2009).

If collimation is not accompanied by significant dissipation, the expanding jet can be described as an ideal relativistic flow confined by a wall that determines the cross section of the jet. Dissipationless collimation conserves entropy, and hence does not change the photon-to-baryon ratio n_γ/n . This implies conservation of the photon number carried by the jet and a constant energy per photon \bar{E} . Collimation boosts the isotropic equivalent of the luminosity L_γ and the isotropic equivalent of the photon flux \dot{N}_γ by the same factor $\sim \theta_c^{-2}$, and their ratio $\bar{E} = L_\gamma/\dot{N}_\gamma$ remains unchanged from its value at r_0 , $\bar{E} = E_0$.

In contrast, dissipative collimation (e.g. involving re-collimation shocks) generates entropy and hence increases n_γ/n . Then the total photon number carried by the jet is increased by a factor of $Q > 1$ and hence \bar{E} (jet energy per photon) is reduced as Q^{-1} , giving a GRB with a reduced E_{pk} .

If there is a relation between θ_c and Q , it leads to a correlated variation of L and E_{pk} (with θ_c being the varying parameter). Thompson et al. (2007) considered the possibility that θ_c always tends to its maximum value $\theta_c \sim \Gamma^{-1}$ allowed by the condition of causal contact across the jet. They pointed out that this gives $\bar{E} \propto \theta_c^{-1}$ and hence $E_{\text{pk}} \propto L^{1/2}$, similar to the observed trend. This simple explanation of the 1/2 slope of the $E_{\text{pk}}-L_\gamma$ correlation is however problematic, as it invokes huge variations in θ_c to cover the observed correlation range, not only from burst to burst but also within a single burst (e.g. Ghirlanda et al. 2011). It also assumes that GRBs of various apparent luminosities $L \sim L_0\theta_c^{-2}$ have approximately the same true power $L_0 \sim 10^{50} \text{ erg s}^{-1}$, which implies a central temperature $kT_0 \approx 1 r_{0,6}^{-1/2} \text{ MeV}$. Then the brightest bursts would have the highest $E_{\text{pk}} \approx 3kT_0 \approx 3 r_{0,6}^{-1/2} \text{ MeV}$, which falls short of the observed highest $E_{\text{pk}} \sim 15 \text{ MeV}$.

Although the dissipative collimation is not the only process regulating the observed E_{pk} (as will be further discussed below), it plays an important role illustrated in Figure 4: beaming/collimation increases the apparent luminosity L_γ while photon production due to dissipation reduces the observed E_{pk} . Reasonable beaming factors $L/L_0 \sim 10^2$ (suggested by the burst energetics and the afterglow data analysis) together with the expected photon production in a dissipative jet naturally explains the location of observed GRBs on the $L_\gamma-E_{\text{pk}}$ diagram.

Evidence for dissipation at small radii and large optical depths is provided by the observed *photon number* emitted in GRBs. In many GRBs, the blackbody central engine is unable to provide the observed photon number, so additional photons must be produced in the expanding jet.

3.2 Planck, Wien, and nonthermal zones below photosphere

Observations also require that dissipation in many GRBs continues at least to the photospheric radius, so that the released spectrum has a nonthermal tail.

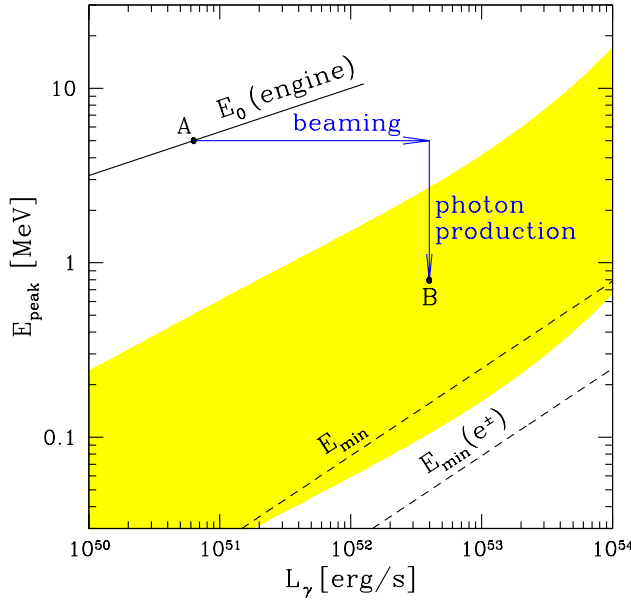


Fig. 4 L_γ - E_{pk} diagram. Point A is an example of the initial condition near the central engine; the jet starts with E_{pk} close to E_0 (Equation 4). As the jet expands, its apparent luminosity L_γ is increased by beaming and E_{pk} is reduced by photon production (dissipation offsets adiabatic cooling). Point B shows the resulting photospheric emission. The approximate region populated by observed GRBs is shown in yellow. The observed E_{pk} should not violate the lower bound E_{min} that is set by the effective blackbody temperature of the photospheric radiation. The dashed lines show E_{min} with and without pair enrichment of the photosphere. (From Beloborodov (2013).)

The effect of dissipation on E_{pk} differs in the following three sub-photospheric zones (Beloborodov 2013).

1. Planck zone ($r \lesssim 10^{10}$ cm, $\tau_T \gtrsim 10^5$): the density of the jet is sufficiently high to maintain blackbody radiation in detailed equilibrium with the thermalized plasma. The thermal plasma efficiently produces photons through double Compton scattering.
2. Wien zone ($\tau_T \gtrsim 10^2$): the dissipated heat is thermalized into a Bose-Einstein photon distribution with a *finite chemical potential*. Kinetic equilibrium between the photons and the plasma is maintained due to the large Kompaneets parameter of the thermal plasma, $y = 4(kT/m_e c^2)\tau_T \gg 1$. The number of photons accumulated in the Wien peak saturates near the Wien radius R_W where y drops to ~ 1 and Comptonization becomes unable to bring new generated photons to the spectral peak.
3. Unsaturated Comptonization zone ($1 \lesssim \tau_T \lesssim 10^2$): heating maintains a Compton parameter $y \sim 1$. The final non-thermal shape of the spectrum is produced in this region. Depending on the details of the dissipation mechanism, the spectrum can develop a high-energy tail up to the GeV band.

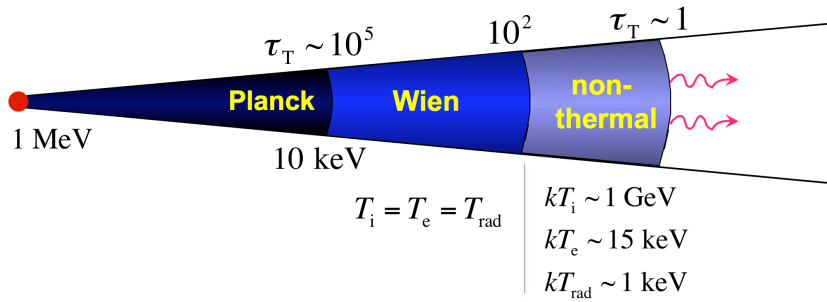


Fig. 5 Three zones in a GRB jet: (1) Planck zone where a blackbody spectrum is enforced; this zone ends where the Thomson optical depth decreases to $\tau_T \approx 10^5$. (2) Wien zone with Kompaneets parameter $y \gg 1$ where radiation has a Bose-Einstein spectrum, and (3) Comptonization (“nonthermal”) zone where the radiation spectrum develops the high-energy tail. In the Planck and Wien zones the ion and electron temperatures are equal to the photon temperature, $T_i = T_e = T_{\text{rad}}$. Outside the Wien zone $T_i \gg T_e \gg T_{\text{rad}}$. The approximate values of the temperatures are indicated in the figure; these characteristic values weakly depend on how the jet is heated. The radiation spectrum is nonthermal in the Comptonization zone and here T_{rad} is defined as the Compton temperature, $T_{\text{rad}} = T_C$ (a measure of the mean photon energy).

In the presence of a soft photon source (synchrotron emission) unsaturated Comptonization also produces a low-energy photon index $\alpha \sim 1$.

Dissipation in the Planck zone reduces E_{pk} . Dissipation in the Wien zone increases E_{pk} if no new photons are produced; strong synchrotron emission in the Wien zone can reduce E_{pk} . In the non-thermal zone E_{pk} remains practically unchanged.

A blackbody photosphere would have the temperature $T = T_{\text{eff}}$ defined by

$$\frac{4}{3} a T_{\text{eff}}^4 \Gamma^2 4\pi R_\star^2 c = L_\gamma. \quad (6)$$

The corresponding E_{pk} would be given by $E_{\text{pk}} \approx 4\Gamma kT_{\text{eff}}$. This estimate should be viewed as a robust lower limit on E_{pk} rather than its true value. One could also define the effective blackbody temperature at the Wien radius, replacing R_\star with R_W in Equation (6) (Giannios 2012). This would still give E_{pk} lower than its true value. A more realistic model should not make the blackbody assumptions at any radii. Instead, it should explicitly follow the production of photons (and their Comptonization) in the expanding jet. Such simulations have been performed recently; their results are described below.

Radiative transfer simulations also give a detailed description of radiation decoupling from the expanding jet. There is no unique sphere of last scattering, and the notion of photosphere is quite fuzzy. R_\star is defined as the radius where $\tau_T = 1$ (see Equation 1). This gives a characteristic decoupling radius, however the location of last scattering is random and surprisingly broadly distributed around R_\star (Pe’er 2008; Beloborodov 2011). 2/3 of photons diffusing from large optical depths are last scattered between $0.3R_\star$ and $3R_\star$, and 1/3 — outside

this interval. Another surprising transfer effect is the significant anisotropy of radiation (measured in the jet rest frame) developing at small radii $r \sim 0.1R_*$ (Beloborodov 2011).

4 GRB spectrum from radiative transfer simulations

Radiation emerging at the photosphere carries information about the entire expansion history of the jet, and the observed spectrum may be used to reconstruct dissipative processes hidden in the opaque region behind the photosphere. This can be achieved by solving a carefully formulated radiative transfer problem, which must be solved consistently with the flow dynamics and heating. A global simulation starting at a sufficiently small radius will show how the jet radiation deviates from blackbody and becomes nonthermal, shaping the observed GRB spectrum.

The effect of subphotospheric heating on GRB radiation has been studied with four different numerical codes (Pe'er et al. 2006; Giannios 2008; Beloborodov 2010; Vurm et al. 2011), consistently giving Band-type spectra. These calculations explored how the spectrum develops the high-energy tail at optical depths $\tau \lesssim 30$ as a result of thermal and nonthermal Comptonization. Recently, Vurm and Beloborodov (2016b) have performed global simulations of radiative transfer starting from very high optical depths $\tau > 10^3$ and including photon production and absorption processes.

4.1 Formulation of the transfer problem

A convenient starting point of transfer simulations is the radius R_c where the collimation process ends and the jet begins to expand conically. The jet is still accelerating at this stage. The acceleration can be self-consistently determined using the dynamical equation (Beloborodov 2011),

$$\frac{d\Gamma}{dr} = \frac{\sigma_T Z_{\pm}}{m_p c^3} F, \quad (7)$$

where F is the radiation flux measured in the plasma rest frame, and Z_{\pm} is the number of electrons and positrons per proton. Equation (7) assumes that radiation pressure dominates the jet acceleration, neglecting the effect of magnetic forces; this approximation may be reasonable even when the jet is strongly magnetized, as long as the jet is hot (Vlahakis and Königl 2003; Russo and Thompson 2013).

Radiation carried by the dissipative jet is influenced by electron heating. Two types of heating should be distinguished: thermal and nonthermal:

- Thermal heating is the energy deposition into the Maxwellian e^{\pm} plasma. In particular, in a two-temperature plasma $T_i \gg T_e$ below the photosphere the electrons are efficiently heated by Coulomb collisions with the hot ions

(Beloborodov 2010). Thermal heating tends to increase the e^\pm temperature above the local Compton temperature of radiation T_C , and the decoupling $T_e > T_C$ becomes significant at $\tau_T \lesssim 10^2$.

- Nonthermal heating is the injection of ultra-relativistic particles with a Lorentz factor γ_{inj} , e.g. by inelastic nuclear collisions ($\gamma_{\text{inj}} \sim m_\pi/m_e \sim 300$) or by other dissipation mechanisms discussed in Section 2. The energetic particles can generate an inverse Compton cascade and their energy is processed into secondary e^\pm pairs of lower energies (Svensson 1987). The value of γ_{inj} is only important for synchrotron emission, which dominates the observed spectrum at $E \ll E_{\text{pk}}$ (see below) and has little relevance to the main MeV peak. Like thermal heating, the main parameter of nonthermal heating is its power.

To keep the number of parameters to a minimum, Vurm and Beloborodov (2016b) employed a simple model of continuous internal dissipation, approximating the thermal and nonthermal dissipation rates as power laws of radius,

$$\frac{dL_{\text{th}}}{d \ln r} = \varepsilon_{0,\text{th}} L \left(\frac{r}{R_c} \right)^{k_{\text{th}}}, \quad \frac{dL_{\text{nth}}}{d \ln r} = \varepsilon_{0,\text{nth}} L \left(\frac{r}{R_c} \right)^{k_{\text{nth}}}, \quad (8)$$

where L is the total energy flow rate in the jet. The power law may be a crude approximation to jet heating by multiple internal shocks or reconnection, however it allows one to study the global picture of the evolution of radiative processes with radius in the expanding jet. The formation of photospheric radiation extends over several decades in radius, and the global simulation allows one to see all stages of this process.

Radiation is described by its intensity $I_\nu(r, \theta, \nu)$ in the fluid frame, where θ is the photon angle with respect to the radial direction. The radiative transfer equation in ultra-relativistic outflows ($\Gamma > 10$) is given by (Beloborodov 2011),

$$\begin{aligned} \frac{1}{r^2 \Gamma} \frac{\partial}{\partial \ln r} [(1 + \mu)r^2 \Gamma I_\nu] &= \frac{r}{\Gamma} (j_\nu - \kappa_\nu I_\nu) + (1 + \mu)(1 - g\mu) \frac{\partial I_\nu}{\partial \ln \nu} \\ &- \frac{\partial}{\partial \mu} [(1 - \mu^2)(1 + \mu) g I_\nu], \end{aligned} \quad (9)$$

where $\mu = \cos \theta$, κ_ν is the opacity, j_ν is the emissivity, and

$$g = 1 - \frac{d \ln \Gamma}{d \ln r}. \quad (10)$$

Equation (9) describes a steady jet, i.e. a simplified model where variability and internal shocks are averaged out and replaced by dissipation terms. At very large optical depths below the photosphere, $\tau_T > 100$, the radiation is approximately isotropic in the fluid frame, which simplifies the transfer problem — it is reduced to advection of isotropic radiation by the expanding outflow. However, a new feature in this region is the importance of induced scattering. Therefore, at $\tau_T > 100$ Equation (9) should be replaced by the Kompaneets equation (see Vurm et al. 2013; Vurm and Beloborodov 2016b).

At optical depths $\tau_T \ll 100$ the radiation becomes significantly anisotropic, and the full transfer Equation (9) should be used; the induced scattering rate is small at these radii and can be neglected.

The radiative transfer is coupled to the evolution of the electron/positron distribution in the expanding jet, which is described by the kinetic equation (Vurm et al. 2011),

$$\begin{aligned} \frac{1}{r^2 \Gamma} \frac{\partial}{\partial \ln r} [r^2 \Gamma n_{\pm}(p)] &= \frac{r}{cI} (j_{\pm} - c\kappa_{\pm} n_{\pm}(p)) \\ - \frac{\partial}{\partial p} \left\{ \frac{r}{cI} \left[\dot{p} n_{\pm}(p) - \frac{1}{2} \frac{\partial}{\partial \gamma} [D n_{\pm}(p)] \right] - \frac{3-g}{3} p n_{\pm}(p) \right\}. \end{aligned} \quad (11)$$

Here $p = \sqrt{\gamma^2 - 1}$ is the electron/positron momentum in units of $m_e c$, and $n_{\pm}(p)$ is the e^{\pm} momentum distribution. The terms \dot{p} and D account for heating/cooling and diffusion in the momentum space due to radiative processes and Coulomb collisions. The emission term j_{\pm} includes the injection of new pairs due to non-thermal dissipation and photon-photon absorption $\gamma + \gamma \rightarrow e^+ + e^-$, and $c\kappa_{\pm} n_{\pm}(p)$ is the pair annihilation rate.

Thermal radiative processes include Comptonization of photons by the thermal plasma, induced Compton scattering at low frequencies, cyclotron emission/absorption, bremsstrahlung, and double Compton scattering. Non-thermal radiative processes result from the injection of relativistic leptons. This leads to the IC e^{\pm} cascade and synchrotron emission, which is an important source of photons. All these processes have been followed in the expanding dissipative jet by Vurm and Beloborodov (2016b) using the exact cross sections and rates and solving numerically the transfer problem described by the coupled Equations (7), (9), (11).

4.2 Main features of sub-photospheric radiative transfer

Figure 6 shows the evolution of the radiation spectrum within a dissipative jet as the jet expands from the highly opaque region $\tau_T \sim 3 \times 10^3$ to transparency. There are two main stages of the spectral evolution:

(1) Generation of photons below the Wien radius ($\tau_T \gtrsim 10^2$) and their Comptonization to the Wien peak. A major source of photons is the synchrotron emission from nonthermal leptons. If the magnetization is relatively weak, e.g. $\varepsilon_B \sim 10^{-2}$, then the synchrotron power is modest, however the *number* of generated photons is substantial, because they are emitted with low energies. Below the Wien radius R_W many of them are Comptonized to the Wien peak and eventually dominate the peak, significantly increasing its photon number and shifting E_{pk} to lower energies. The decrease of E_{pk} due to the continuing photon supply to the peak ends when τ_T is reduced below $\sim 10^2$, which approximately corresponds to R_W .

(2) Broadening of the spectrum by unsaturated Comptonization outside the Wien radius, leading to a nonthermal shape of the spectrum. The thermal Comptonization gradually switches to the unsaturated regime at $r \sim R_W$

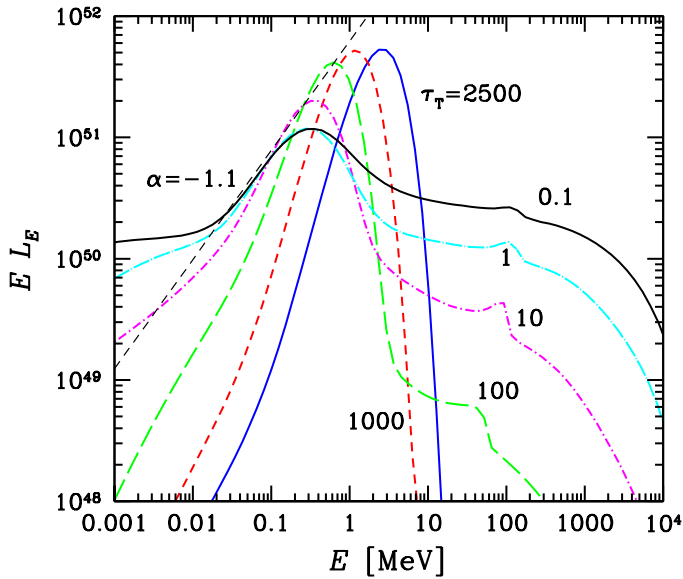


Fig. 6 Evolution of the radiation spectrum carried by the jet from high to low optical depths τ_T in a sample model with $L = 2 \times 10^{52}$ erg/s, $\eta = 190$, and $\epsilon_B = \sigma/2 = 10^{-2}$. The simulation started at radius $R_c = 10^{11}$ cm with $\Gamma_c = 20$, and the jet was continually heated with $\epsilon_{th} = \epsilon_{nth} = 0.025$. The spectra are measured in the rest frame of the central engine and not corrected for a cosmological redshift. The black curve ($\tau_T = 0.1$) shows the observed (escaping) spectrum that result from this evolution. (From Vurm and Beloborodov (2016b).)

and then the Compton y -parameter stays near unity. The production of synchrotron photons continues at $r > R_W$ and results in the soft “excess” seen below a few $\times 10$ keV in the emitted spectrum (Figure 6). More importantly, unsaturated Comptonization of these photons plays a key role in determining the spectral slope α below the peak. The slope begins to soften near the Wien radius and attains its final value $\alpha \sim -1$ near the photosphere. The value of α depends on the heating history at $r > R_W$, in particular on the nonthermal dissipation channel, and is expected to vary, however $\alpha \sim -1$ is a characteristic signature of unsaturated Comptonization.

The high-energy tail of the spectrum develops mostly near the photosphere, due to two effects, thermal and nonthermal. Outside the Wien radius the electron temperature rises significantly above E_{pk}/Γ and thermal Comptonization begins to produce photons with energies $E > E_{pk}$. As the optical depth drops, the nonthermal high-energy component becomes increasingly prominent, especially in weakly magnetized jets with the dominant IC cooling. Then the overlapping thermal and nonthermal Comptonization components together form an extended high-energy spectrum, which may superficially appear as a single emission component.

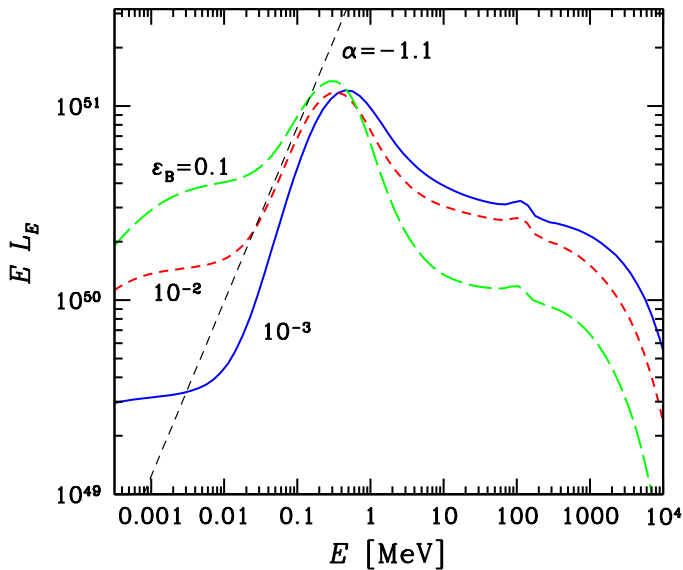


Fig. 7 Effect of varying magnetization on the emerging spectrum (Vurm and Beloborodov 2016b). If variations of ε_B are not resolved, a superposition of the spectra will be observed.

As seen in Figure 6, the spectrum has a distinctly nonthermal shape already well below the photosphere (at $\tau_T \gtrsim 10$). In particular, the low-energy slope is significantly softer than the Planck (or Wien) spectrum. Even if dissipation stopped completely at $\tau_T \sim 10$, a thermal-looking prompt emission would not be expected; instead, the emerging spectrum would resemble an exponentially cutoff power law.

The dependence of the photospheric spectrum on the jet magnetization ε_B is shown in Figure 7. Very weak magnetization $\varepsilon_B < 10^{-3}$ is disfavored for typical GRBs, as it leads to a hard slope α at low energies — then practically the entire spectrum is dominated by the Comptonized photons advected from very large optical depths, with little photon production at moderate τ_T . The preferred magnetization is in the range $10^{-3} < \varepsilon_B < 0.1$, which gives α varying around -1 . At the low- ε_B end, the nonthermal e^\pm cascades are particularly efficient, and the pairs outnumber protons on average by a factor of $\gtrsim 10$.

A large fraction of produced pairs “freeze out” in the expanding jet, so the jet remains forever dominated by e^\pm pairs. This should affect the afterglow emission produced by the reverse shock when the jet interacts with the external medium. Thus, the reverse-shock component in a GRB afterglow could serve as a probe of pair loading.

In strongly magnetized jets with $\varepsilon_B \gtrsim 1$, the pair cascade and nonthermal Comptonization are suppressed, leading to a different radiation spectrum at high energies (Vurm et al. 2011). Radiation from magnetically dominated jets was recently considered by Gill and Thompson (2014); Thompson and Gill

(2014) and Bégué and Pe’er (2015). Gill and Thompson envision a two-stage evolution of a jet that starts out baryon-free and dominated by the Poynting flux. In their scenario, baryon loading occurs at a large radius, and the jet opacity is dominated by electron-positron pairs generated by dissipation, which takes place in two separate episodes. Despite the complicated details, the evolution of radiative processes in their picture resembles that shown in Figure 6 — basically, generation of synchrotron photons at large optical depths is followed by Comptonization into a Band-like spectrum.

4.3 Comparison with observed spectra

A continuously heated and moderately magnetized jet generates a Band-type photospheric spectrum, with spectral slopes α , β , and peak position E_{pk} consistent with observations. The radiative transfer simulations show a moderate dependence of E_{pk} on the parameters of the problem, and no fine-tuning is needed to bring the peak into the observed range around 1 MeV.

A typical burst with $L \approx 10^{52}$ erg/s, a canonical Band spectrum, and $E_{\text{pk}} \lesssim 1$ MeV is reproduced by the model if:

1. The jet magnetization is in the range $10^{-3} < \varepsilon_{\text{B}} < 0.1$. Very weak magnetization increases E_{pk} by suppressing synchrotron emission; strong magnetization softens the spectrum both below and above the peak, and generates a prominent soft “excess” below a few tens of keV.
2. The jet Lorentz factor $\Gamma(R_{\text{c}}) = 10 - 100$ at radii comparable to that of the stellar progenitor. Jets with a low $\Gamma(R_{\text{c}})$ are more “photon-rich” and produce GRBs with low E_{pk} .
3. Heating has a nonthermal component that injects relativistic leptons into the jet. The subphotospheric nonthermal particles play a key role by providing soft synchrotron photons as seeds for Comptonization. This impacts the formation of both E_{pk} (at $\tau_{\text{T}} \gtrsim 10^2$) and slope α (at $1 < \tau < 10^2$). The absence of nonthermal leptons would lead to hard spectra with high E_{pk} .

The detailed radiative transfer models have been applied to three well-studied bright bursts, GRB 990123, GRB 090902B, and GRB 130427A, which show different prompt spectra, and successful fits have been found in all three cases (Vurm and Beloborodov 2016b). The fits gave estimates for the main parameters of the GRB jets (Table 1). In particular, the best-fit magnetization varies between 0.01 and 0.1, and the final Lorentz factor Γ_f between 300 and 1200. The corresponding photospheric radius R_{\star} varies around 10^{13} cm.

The obtained Γ_f can be compared with the results of another, independent method of estimating the jet Lorentz factor. This method is based on the reconstruction of the GeV+optical flash produced by the jet at much larger radii $r \gtrsim 10^{16}$ cm where it drives the external blast wave (Beloborodov et al. 2014; Vurm et al. 2014; Hascoët et al. 2015). Remarkably, the prompt emission fit for GRB 130427A gave $\Gamma_{\text{f}} \approx 300$, close to the ejecta Lorentz factor $\Gamma_{\text{ej}} \approx 350$ obtained from the GeV+optical flash reconstruction (Vurm et al. 2014).

Table 1 Jet parameters for three fitted GRBs (from Vurm and Beloborodov (2016b)).

GRB	L_{54}	Γ_c	Γ_f	ε_B	$\epsilon_{0,\text{th}}$	$\epsilon_{0,\text{nth}}$
990123	0.44	35	500	0.018	0.099	0.021
090902B	2.3	70	1220	0.012	0.055	0.065
130427A	0.47	64	300	0.046	0.093	0.067

The fit to GRB 090902B gave $\Gamma_f \approx 1200$, which is higher than $\Gamma_{\text{ej}} = 600 - 900$ used to fit the GeV flash. However, in this case there is no significant inconsistency, because the reverse shock in the blast wave from GRB 090902B is relativistic; in this case the flash modeling only gives a lower limit $\Gamma_{\text{ej}} > 600$ (Hascoët et al. 2015). A similar $\Gamma \approx 1000$ was proposed by Pe’Er et al. (2012) based on a different phenomenological model for GRB 090902B (a multicolor blackbody for the photosphere and nonthermal radiation from dissipation at a large radius).

Besides the values of Γ and ε_B , the radiative transfer models of the prompt emission give insights into the heating history of the GRB jets. The fit to GRB 130427A requires that the nonthermal heating be significantly deep below the photosphere and become weak well before the jet expands to transparency; the observed Band-like spectrum is mainly shaped by thermal Comptonization. In GRB 990123, thermal heating appears to dominate at all radii, and the nonthermal synchrotron source is relatively weak. The model still predicts a moderate excess below a few tens of keV due to synchrotron emission. A hint of such excess is indeed seen in the data (Figure 2 in Briggs et al. (1999); R. Preece, private communication).

In contrast, nonthermal dissipation in GRB 090902B is found to be strong up to the photosphere and beyond. It explains the observed high-energy component and the soft excess, which were previously modeled as a power law of unknown origin (Abdo and the Fermi collaboration 2009). The two models are compared in Figure 8. The radiative transfer model shows that the soft excess is the synchrotron emission and the high-energy component is IC emission from nonthermal electrons.² They are not parts of a single power law, however they are produced by the same nonthermal electron population. The high-energy component of the prompt emission is also expected to contaminate (at early times) the GeV flash observed in GRB 090902B by *Fermi* LAT.

5 Polarization

Linear polarization measurements in the hard X-ray band have been reported for GRB 041219A (Kalemci et al. 2007; McGlynn et al. 2007; Götz et al. 2009), GRB 061122 (McGlynn et al. 2009; Götz et al. 2013), GRB 100826A (Yonetoku et al. 2011), GRB 110301A, GRB 110721A (Yonetoku et al. 2012), and GRB 140206A (Götz et al. 2014). However, the detection significance for

² A different hadronic shock model explanation was also proposed by Asano et al. (2010)

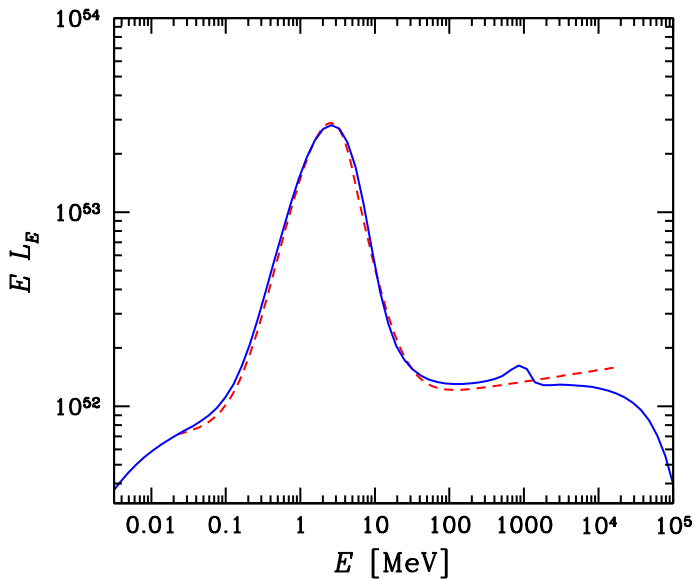


Fig. 8 Radiative transfer model for GRB 090902B (solid curve). The dashed curve shows the Band+power-law fit by Abdo and the Fermi collaboration (2009), in time bin b. (From Vurm and Beloborodov (2016b)).

all these bursts is modest, because of a low sensitivity, and the measurements have poorly known systematic uncertainties. Future detectors can significantly improve the polarization information, which will be highly valuable for GRB modeling.

Radiative transfer in the jet occurs in two linear polarization states with different intensities, however this gives no observable polarization as long as the emission is symmetric about the line of sight (Beloborodov 2011). Due to the radial Doppler beaming of radiation, the observed GRB radiation is expected to come from a narrow region around the line of sight, of angular size $\delta\theta \sim \Gamma^{-1}$. Its symmetry can be broken in two ways.

(1) A preferred direction for polarization appears if there is a strong transverse gradient in the jet parameters at the photosphere (e.g. a gradient in luminosity, Lorentz factor, etc.). Then observable polarization emerges after the last scattering around R_* , which was investigated by Lundman et al. (2014) and Ito et al. (2014). They predicted polarization degrees up to $\Pi \sim 40\%$ if the jet has significant structure on angular scales $\delta\theta \sim \Gamma^{-1}$. In particular, a strong transverse gradient is expected near the jet edge $\theta = \theta_c$. If the collimation angle θ_c is not much larger than Γ^{-1} then observers detecting a bright burst (but not exactly on the jet axis) will see the jet cross section $\sim \pi r^2 \theta_c^2$ at some inclination. Then the line of sight and the jet axis form a preferred plane and a strong linear polarization should show up in the main peak of the GRB spectrum. Lundman et al. (2014) also showed that for a jet with $\theta_c \gg \Gamma^{-1}$

the probability to observe its edge (and hence to break the symmetry of observed emission) is $\sim 4(\Gamma\theta_c)^{-1}$. For instance, if $\theta_c \sim 0.1$ and $\Gamma \approx 400$ the edge should be visible in roughly 10% of detected GRBs. The actual distribution of θ_c is however unknown; attempts to infer this distribution from the analysis of so-called “jet breaks” in afterglow light curves have been inconclusive.

(2) If part of the GRB spectrum is dominated by synchrotron radiation, a preferred direction for polarization can be set by the magnetic field where this radiation is produced. The transfer models discussed in Section 4 show that the main MeV peak is dominated by the Comptonized radiation advected from large optical depths. The Comptonized peak is unpolarized as long as there is no significant structure on angular scales $\delta\theta \sim \Gamma^{-1}$. However, at sufficiently low energies $E \ll E_{\text{pk}}$ the spectrum is dominated by synchrotron emission. This leads to a unique polarization signature: a rise in GRB polarization toward lower energies (Lundman et al. 2016).

Synchrotron emission from relativistic electrons in a uniform magnetic field \mathbf{B} is linearly polarized in the plane perpendicular to \mathbf{B} . The polarization degree for an isotropic electron distribution is $\Pi_{\text{syn}} = (p+1)/(p+7/3)$, where $p = d \ln N / d \ln E_e$ is the slope of the electron spectrum (e.g. Rybicki and Lightman 1979). This standard result is somewhat modified when the observed region is a spherical patch in a relativistic outflow, carrying an ordered transverse magnetic field, which gives Π_{syn} varying around 50%, depending on p (Lyutikov et al. 2003). Synchrotron radiation produced well below the photosphere will lose its polarization after a few scatterings, however a significant fraction of synchrotron photons produced around and above the photosphere will escape without scattering and preserve their polarization. The observed GRB spectrum $L(E)$ can be viewed as the sum of two contributions: photons escaping the jet after their last Compton scattering, $L_{\text{sc}}(E)$, and photons escaping directly after their emission by the synchrotron mechanism, with no scattering, $L_{\text{nsc}}(E)$. The observed polarization is then given by

$$\Pi(E) = f_{\text{nsc}}(E)\Pi_{\text{syn}}, \quad f_{\text{nsc}}(E) = \frac{L_{\text{nsc}}(E)}{L(E)}. \quad (12)$$

Using the transfer models of Vurm and Beloborodov (2016b), Lundman et al. (2016) calculated $f_{\text{nsc}}(E)$ and the expected polarization degree $\Pi(E)$ for GRBs 990123, 090902B, and 110721A. Their results demonstrate that strong polarization is expected in the X-ray band under two conditions: (1) significant dissipation extends to $r \gtrsim R_*$ and is accompanied by injection of nonthermal particles, and (2) the jet magnetization is significant, $\varepsilon_B \gtrsim 10^{-2}$. These conditions are well satisfied in GRB 090902B (Section 4). Then the GRB spectrum has a prominent soft excess emerging above the Band spectrum at low energies, and a significant fraction of this excess is formed by unscattered synchrotron photons. This leads to the strong polarization rise toward low energies (Figure 9).

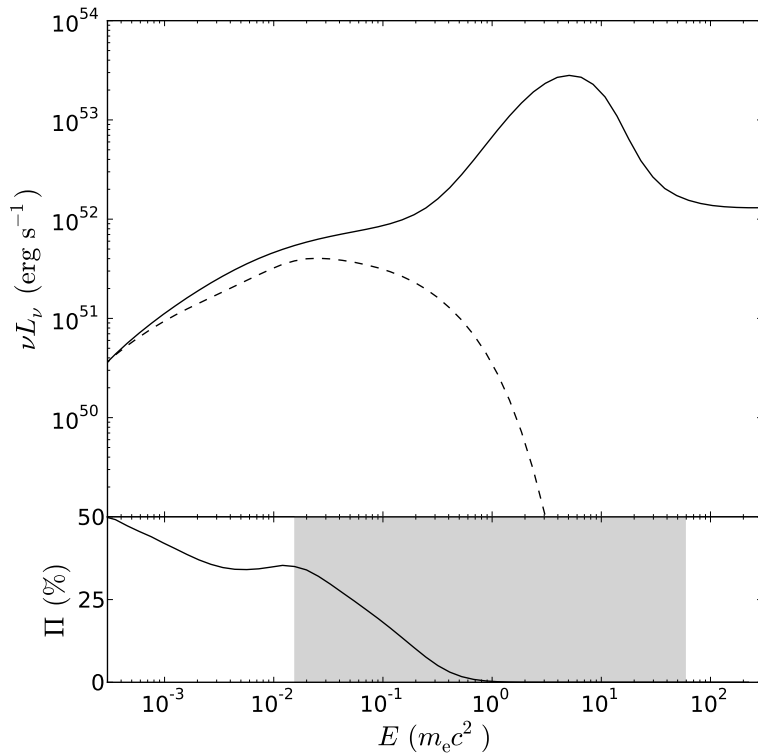


Fig. 9 Top panel: the simulated spectrum of GRB 090902B (solid curve) and the contribution of unscattered synchrotron emission (dashed curve). Their ratio gives the unscattered fraction $f_{\text{nsc}}(E)$. Bottom panel: expected polarization as a function of photon energy E . The shaded region shows the Fermi GBM band (NaI + BGO detectors, 8 keV to 30 MeV). (From Lundman et al. (2016).)

6 Possible future developments

The detailed radiative transfer simulations can be systematically applied to all available spectra of prompt GRB emission, including those resolved in time. Such fits would reconstruct the jet heating and magnetization for a large sample of GRBs and may reveal important correlations. This could shed light on how the jets are produced and heated, and what role is played in this process by the magnetic field.

The analysis of prompt emission can be combined with that of GRB afterglow, especially its early phase. The GeV+optical flash predicted and observed at the onset of the afterglow (Beloborodov et al. 2014) provides particularly useful data that recently helped to disentangle the main parameters of the blast wave in seven GRBs (Hascoët et al. 2015). The initial Lorentz factor of the blast wave reconstructed by this method can be compared with the jet Lorentz factor inferred from the transfer simulations of the prompt emission,

as has been done for GRB 130427A. An additional test would be provided by future detections of the predicted TeV counterpart of the GeV+optical flash, which should rise with some delay (Hascoët et al. 2015). It is detectable by current ground-based Cherenkov telescopes and should certainly be detected by the future Cherenkov Telescope Array (CTA) (Vurm and Beloborodov 2016a).

Spectra of prompt GRB emission are poorly known at low energies, from soft X-rays to the optical band. While the main MeV peak is dominated by the Comptonized radiation advected from large optical depths, the prompt optical radiation must be dominated by synchrotron emission outside the scattering photosphere. The low-frequency emission is predicted to be affected by synchrotron self-absorption, which tends to give a flat spectral slope (Vurm et al. 2011). While prompt optical emission has been detected in some GRBs, there is currently no information on its spectral slope. A color measurement and better sampling of the optical light curve would provide useful information about dissipation outside the photosphere and inside of the external blast wave. This is a rather broad range of radii, even taking into account that the photosphere can be “carried” forward by the e^\pm -dressed internal shocks up to two decades in radius (Section 2). Radiation produced outside the photosphere is expected to have a broad nonthermal spectrum with no sharp MeV peak and a slower variability on timescales $\sim r/c\Gamma^2$.

Important developments may result from future observations of polarization of the prompt GRB emission and its variation across the burst spectrum. An unpolarized MeV peak and a rise in linear polarization toward low photon energies would confirm the synchrotron contribution at $E \ll E_{\text{pk}}$ predicted by the radiative transfer simulations (Sections 4 and 5). Bursts similar to GRB 090902B are the most promising targets for such observations. Observations of polarization of the main MeV peak of photospheric emission would provide evidence for a transverse structure of the jet on angular scales $\delta\theta \sim \Gamma^{-1}$.

Detection of neutrinos from GRB explosions is possible in the near future. The detection (or strong upper limits) would test the ideas for the dissipation mechanism in the relativistic jet, including that in the opaque region well below the photosphere. In particular, the expected presence of a free neutron component leads to strong nuclear collisional dissipation, which produces 10–100 GeV neutrinos detectable by IceCube DeepCore.

Acknowledgements AMB’s research is supported by NSF grant AST-1412485, NASA grant NNX15AE26G, and a grant from the Simons Foundation (#446228, Andrei Beloborodov). PM’s research is supported by NASA grant NNX13AH50G.

References

- A.A. Abdo, the Fermi collaboration, Fermi Observations of GRB 090902B: A Distinct Spectral Component in the Prompt and Delayed Emission. *Astrophys.J.Lett.* **706**, 138–144 (2009). doi:10.1088/0004-637X/706/1/L138

- M. Ackermann, The Fermi collaboration, Multiwavelength Observations of GRB 110731A: GeV Emission from Onset to Afterglow. *Astrophys.J.* **763**, 71 (2013). doi:10.1088/0004-637X/763/2/71
- K. Asano, S. Inoue, P. Mészáros, Prompt X-ray and Optical Excess Emission Due to Hadronic Cascades in Gamma-ray Bursts. *Astrophys.J.Lett.* **725**, 121–125 (2010). doi:10.1088/2041-8205/725/2/L121
- M. Axelsson, L. Borgonovo, The width of gamma-ray burst spectra. *M.N.R.A.S.* **447**, 3150–3154 (2015). doi:10.1093/mnras/stu2675
- J.N. Bahcall, P. Mészáros, 5–10 GeV Neutrinos from Gamma-Ray Burst Fireballs. *Physical Review Letters* **85**, 1362–1365 (2000)
- D.L. Band, M. Axelsson, L. Baldini, G. Barbiellini, M.G. Baring, D. Bastieri, M. Battelino, R. Bellazzini, E. Bissaldi, G. Bogaert, J. Bonnell, J. Chiang, J. Cohen-Tanugi, V. Connaughton, S. Cutini, F. de Palma, B.L. Dingus, E. do Couto e Silva, G. Fishman, A. Galli, N. Gehrels, N. Giglietto, J. Granot, S. Guiriec, R.E. Hughes, T. Kamae, N. Komin, F. Kuehn, M. Kuss, F. Longo, P. Lubrano, R.M. Kippen, M.N. Mazziotta, J.E. McEnery, S. McGlynn, E. Moretti, T. Nakamori, J.P. Norris, M. Ohno, M. Olivo, N. Omodei, V. Pelassa, F. Piron, R. Preece, M. Razzano, J.J. Russell, F. Ryde, P.M. Saz Parkinson, J.D. Scargle, C. Sgrò, T. Shimokawabe, P.D. Smith, G. Spandre, P. Spinelli, M. Stamatikos, B.L. Winer, R. Yamazaki, Prospects for GRB Science with the Fermi Large Area Telescope. *Astrophys.J.* **701**, 1673–1694 (2009). doi:10.1088/0004-637X/701/2/1673
- I. Bartos, A.M. Beloborodov, K. Hurley, S. Márka, Detection Prospects for GeV Neutrinos from Collisionally Heated Gamma-ray Bursts with IceCube/DeepCore. *Physical Review Letters* **110**(24), 241101 (2013). doi:10.1103/PhysRevLett.110.241101
- D. Bégué, A. Pe’er, Poynting-flux-dominated Jets Challenged by their Photospheric Emission. *Astrophys.J.* **802**, 134 (2015). doi:10.1088/0004-637X/802/2/134
- A.M. Beloborodov, Nuclear Composition of Gamma-Ray Burst Fireballs. *Astrophys.J.* **588**, 931–944 (2003). doi:10.1086/374217
- A.M. Beloborodov, Collisional mechanism for gamma-ray burst emission. *M.N.R.A.S.* **407**, 1033–1047 (2010). doi:10.1111/j.1365-2966.2010.16770.x
- A.M. Beloborodov, Radiative Transfer in Ultrarelativistic Outflows. *Astrophys.J.* **737**, 68 (2011). doi:10.1088/0004-637X/737/2/68
- A.M. Beloborodov, Regulation of the Spectral Peak in Gamma-Ray Bursts. *Astrophys.J.* **764**, 157 (2013). doi:10.1088/0004-637X/764/2/157
- A.M. Beloborodov, Sub-photospheric shocks in relativistic explosions. *ArXiv e-prints* **1604.02794** (2016)
- A.M. Beloborodov, R. Hascoët, I. Vurm, On the Origin of GeV Emission in Gamma-Ray Bursts. *Astrophys.J.* **788**, 36 (2014). doi:10.1088/0004-637X/788/1/36
- A.M. Beloborodov, B.E. Stern, R. Svensson, Power Density Spectra of Gamma-Ray Bursts. *Astrophys.J.* **535**, 158–166 (2000). doi:10.1086/308836
- R.D. Blandford, D.G. Payne, Compton Scattering in a Converging Fluid Flow - Part Two - Radiation Dominated Shock. *M.N.R.A.S.* **194**, 1041 (1981). doi:10.1093/mnras/194.4.1041
- M.S. Briggs, D.L. Band, R.M. Kippen, R.D. Preece, C. Kouveliotou, J. van Paradijs, G.H. Share, R.J. Murphy, S.M. Matz, A. Connors, C. Winkler, M.L. McConnell, J.M. Ryan, O.R. Williams, C.A. Young, B. Dingus, J.R. Catelli, R.A.M.J. Wijers, Observations of GRB 990123 by the Compton Gamma Ray Observatory. *Astrophys.J.* **524**, 82–91 (1999). doi:10.1086/307808
- O. Bromberg, A. Levinson, Recollimation and Radiative Focusing of Relativistic Jets: Applications to Blazars and M87. *Astrophys.J.* **699**, 1274–1280 (2009). doi:10.1088/0004-637X/699/2/1274
- O. Bromberg, J. Granot, T. Piran, On the composition of GRBs’ Collapsar jets. *M.N.R.A.S.* **450**, 1077–1084 (2015). doi:10.1093/mnras/stv226
- R. Budnik, B. Katz, A. Sagiv, E. Waxman, Relativistic Radiation Mediated Shocks. *Astrophys.J.* **725**, 63–90 (2010). doi:10.1088/0004-637X/725/1/63
- J.M. Burgess, R.D. Preece, M.G. Baring, M.S. Briggs, V. Connaughton, S. Guiriec, W.S. Paciesas, C.A. Meegan, P.N. Bhat, E. Bissaldi, V. Chaplin, R. Diehl, G.J. Fishman, G. Fitzpatrick, S. Foley, M. Gibby, M. Giles, A. Goldstein, J. Greiner, D. Gruber, A.J.

- van der Horst, A. von Kienlin, M. Kippen, C. Kouveliotou, S. McBreen, A. Rau, D. Tierney, C. Wilson-Hodge, Constraints on the Synchrotron Shock Model for the Fermi GRB 090820A Observed by Gamma-Ray Burst Monitor. *Astrophys.J.* **741**, 24 (2011). doi:10.1088/0004-637X/741/1/24
- J.M. Burgess, R.D. Preece, F. Ryde, P. Veres, P. Mészáros, V. Connaughton, M. Briggs, A. Pe’er, S. Iyyani, A. Goldstein, M. Axelsson, M.G. Baring, P.N. Bhat, D. Byrne, G. Fitzpatrick, S. Foley, D. Kocevski, N. Omodei, W.S. Paciesas, V. Pelassa, C. Kouveliotou, S. Xiong, H.-F. Yu, B. Zhang, S. Zhu, An Observed Correlation between Thermal and Non-thermal Emission in Gamma-Ray Bursts. *Astrophys.J.Lett.* **784**, 43 (2014). doi:10.1088/2041-8205/784/2/L43
- F. Daigne, R. Mochkovitch, Gamma-ray bursts from internal shocks in a relativistic wind: temporal and spectral properties. *M.N.R.A.S.* **296**, 275–286 (1998). doi:10.1046/j.1365-8711.1998.01305.x
- E.V. Derishev, V.V. Kocharovskiy, V.V. Kocharovskiy, The Neutron Component in Fireballs of Gamma-Ray Bursts: Dynamics and Observable Imprints. *Astrophys.J.* **521**, 640–649 (1999). doi:10.1086/307574
- E.V. Derishev, F.A. Aharonian, V.V. Kocharovskiy, V.V. Kocharovskiy, Particle acceleration through multiple conversions from a charged into a neutral state and back. *Phys.Rev.D* **68**(4), 043003 (2003). doi:10.1103/PhysRevD.68.043003
- G. Drenkhahn, H.C. Spruit, Efficient acceleration and radiation in Poynting flux powered GRB outflows. *Astron.Astrophys.* **391**, 1141–1153 (2002). doi:10.1051/0004-6361:20020839
- D. Eichler, A. Levinson, A Compact Fireball Model of Gamma-Ray Bursts. *Astrophys.J.* **529**, 146–150 (2000). doi:10.1086/308245
- G. Ghirlanda, L. Nava, G. Ghisellini, A. Celotti, D. Burlon, S. Covino, A. Melandri, Gamma-ray bursts in the comoving frame. *M.N.R.A.S.* **420**, 483–494 (2012). doi:10.1111/j.1365-2966.2011.20053.x
- G. Ghisellini, Blazars and Gamma Ray Bursts, in *VI Microquasar Workshop: Microquasars and Beyond*, 2006, pp. 27–31
- G. Giacinti, A.R. Bell, Collisionless shocks and TeV neutrinos before Supernova shock breakout from an optically thick wind. *M.N.R.A.S.* **449**, 3693–3699 (2015). doi:10.1093/mnras/stv561
- D. Giannios, Prompt GRB emission from gradual energy dissipation. *Astron.Astrophys.* **480**, 305–312 (2008). doi:10.1051/0004-6361:20079085
- D. Giannios, The peak energy of dissipative gamma-ray burst photospheres. *M.N.R.A.S.* **422**, 3092–3098 (2012). doi:10.1111/j.1365-2966.2012.20825.x
- D. Giannios, H.C. Spruit, Spectral and timing properties of a dissipative gamma-ray burst photosphere. *Astron.Astrophys.* **469**, 1–9 (2007). doi:10.1051/0004-6361:20066739
- R. Gill, C. Thompson, Non-thermal Gamma-Ray Emission from Delayed Pair Breakdown in a Magnetized and Photon-rich Outflow. *Astrophys.J.* **796**, 81 (2014). doi:10.1088/0004-637X/796/2/81
- A. Goldstein, J.M. Burgess, R.D. Preece, M.S. Briggs, S. Guiriec, A.J. van der Horst, V. Connaughton, C.A. Wilson-Hodge, W.S. Paciesas, C.A. Meegan, A. von Kienlin, P.N. Bhat, E. Bissaldi, V. Chaplin, R. Diehl, G.J. Fishman, G. Fitzpatrick, S. Foley, M. Gibby, M. Giles, J. Greiner, D. Gruber, R.M. Kippen, C. Kouveliotou, S. McBreen, S. McGlynn, A. Rau, D. Tierney, The Fermi GBM Gamma-Ray Burst Spectral Catalog: The First Two Years. *Astrophys.J.Supp.* **199**, 19 (2012). doi:10.1088/0067-0049/199/1/19
- J. Goodman, Are gamma-ray bursts optically thick? *Astrophys.J.Lett.* **308**, 47–50 (1986). doi:10.1086/184741
- D. Götz, P. Laurent, F. Lebrun, F. Daigne, Ž. Bošnjak, Variable Polarization Measured in the Prompt Emission of GRB 041219A Using IBIS on Board INTEGRAL. *Astrophys.J.Lett.* **695**, 208–212 (2009). doi:10.1088/0004-637X/695/2/L208
- D. Götz, S. Covino, A. Fernández-Soto, P. Laurent, Ž. Bošnjak, The polarized gamma-ray burst GRB 061122. *M.N.R.A.S.* **431**, 3550–3556 (2013). doi:10.1093/mnras/stt439
- D. Götz, P. Laurent, S. Antier, S. Covino, P. D’Avanzo, V. D’Elia, A. Melandri, GRB 140206A: the most distant polarized gamma-ray burst. *M.N.R.A.S.* **444**, 2776–2782 (2014). doi:10.1093/mnras/stu1634
- R. Hascoët, I. Vurm, A.M. Beloborodov, Measuring Ambient Densities and Lorentz Fac-

- tors of Gamma-Ray Bursts from GeV and Optical Observations. *Astrophys.J.* **813**, 63 (2015). doi:10.1088/0004-637X/813/1/63
- H. Ito, S. Nagataki, J. Matsumoto, S.-H. Lee, A. Tolstov, J. Mao, M. Dainotti, A. Mizuta, Spectral and Polarization Properties of Photospheric Emission from Stratified Jets. *Astrophys.J.* **789**, 159 (2014). doi:10.1088/0004-637X/789/2/159
- H. Ito, J. Matsumoto, S. Nagataki, D.C. Warren, M.V. Barkov, Photospheric Emission from Collapsar Jets in 3D Relativistic Hydrodynamics. *Astrophys.J.Lett.* **814**, 29 (2015). doi:10.1088/2041-8205/814/2/L29
- D. Kagan, L. Sironi, B. Cerutti, D. Giannios, Relativistic Magnetic Reconnection in Pair Plasmas and Its Astrophysical Applications. *SSRv.* **191**, 545–573 (2015). doi:10.1007/s11214-014-0132-9
- E. Kalemci, S.E. Boggs, C. Kouveliotou, M. Finger, M.G. Baring, Search for Polarization from the Prompt Gamma-Ray Emission of GRB 041219a with SPI on INTEGRAL. *Astrophys.J.Supp.* **169**, 75–82 (2007). doi:10.1086/510676
- Y. Kaneko, R.D. Preece, M.S. Briggs, W.S. Paciesas, C.A. Meegan, D.L. Band, The Complete Spectral Catalog of Bright BATSE Gamma-Ray Bursts. *Astrophys.J.Supp.* **166**, 298–340 (2006). doi:10.1086/505911
- K. Kashiyama, K. Murase, P. Mészáros, Neutron-Proton-Converter Acceleration Mechanism at Subphotospheres of Relativistic Outflows. *Physical Review Letters* **111**(13), 131103 (2013). doi:10.1103/PhysRevLett.111.131103
- S. Kobayashi, T. Piran, R. Sari, Can Internal Shocks Produce the Variability in Gamma-Ray Bursts? *Astrophys.J.* **490**, 92 (1997)
- S.S. Komissarov, N. Vlahakis, A. Königl, M.V. Barkov, Magnetic acceleration of ultrarelativistic jets in gamma-ray burst sources. *M.N.R.A.S.* **394**, 1182–1212 (2009). doi:10.1111/j.1365-2966.2009.14410.x
- D. Lazzati, B.J. Morsony, M.C. Begelman, Very High Efficiency Photospheric Emission in Long-Duration γ -Ray Bursts. *Astrophys.J.Lett.* **700**, 47–50 (2009). doi:10.1088/0004-637X/700/1/L47
- D. Lazzati, M. Villeneuve, D. Lopez-Camara, B. Morsony, R. Perna, On the observed duration distribution of gamma-ray bursts from collapsars. *ArXiv e-prints* (2013)
- A. Levinson, Observational Signatures of Sub-photospheric Radiation-mediated Shocks in the Prompt Phase of Gamma-Ray Bursts. *Astrophys.J.* **756**, 174 (2012). doi:10.1088/0004-637X/756/2/174
- A. Levinson, O. Bromberg, Relativistic Photon Mediated Shocks. *Physical Review Letters* **100**(13), 131101 (2008). doi:10.1103/PhysRevLett.100.131101
- C. Lundman, A. Pe’er, F. Ryde, Polarization properties of photospheric emission from relativistic, collimated outflows. *M.N.R.A.S.* **440**, 3292–3308 (2014). doi:10.1093/mnras/stu457
- C. Lundman, I. Vurm, A.M. Beloborodov, Polarization of gamma-ray bursts in the dissipative photosphere model. *ArXiv e-prints* (2016)
- M. Lyutikov, V.I. Pariev, R.D. Blandford, Polarization of Prompt Gamma-Ray Burst Emission: Evidence for Electromagnetically Dominated Outflow. *Astrophys.J.* **597**, 998–1009 (2003). doi:10.1086/378497
- S. McGlynn, D.J. Clark, A.J. Dean, L. Hanlon, S. McBreen, D.R. Willis, B. McBreen, A.J. Bird, S. Foley, Polarisation studies of the prompt gamma-ray emission from GRB 041219a using the spectrometer aboard INTEGRAL. *Astron.Astrophys.* **466**, 895–904 (2007). doi:10.1051/0004-6361:20066179
- S. McGlynn, S. Foley, B. McBreen, L. Hanlon, S. McBreen, D.J. Clark, A.J. Dean, A. Martin-Carrillo, R. O’Connor, High energy emission and polarisation limits for the INTEGRAL burst GRB 061122. *Astron.Astrophys.* **499**, 465–472 (2009). doi:10.1051/0004-6361/200810920
- P. Mészáros, M.J. Rees, Multi-GeV Neutrinos from Internal Dissipation in Gamma-Ray Burst Fireballs. *Astrophys.J.Lett.* **541**, 5–8 (2000a). doi:10.1086/312894
- P. Mészáros, M.J. Rees, Steep Slopes and Preferred Breaks in Gamma-Ray Burst Spectra: The Role of Photospheres and Comptonization. *Astrophys.J.* **530**, 292–298 (2000b). doi:10.1086/308371
- P. Mészáros, E. Waxman, TeV Neutrinos from Successful and Choked Gamma-Ray Bursts. *Physical Review Letters* **87**(17), 171102 (2001)

- B.J. Morsony, D. Lazzati, M.C. Begelman, The Origin and Propagation of Variability in the Outflows of Long-duration Gamma-ray Bursts. *Astrophys.J.* **723**, 267–276 (2010). doi:10.1088/0004-637X/723/1/267
- K. Murase, K. Kashiyama, P. Mészáros, Subphotospheric Neutrinos from Gamma-Ray Bursts: The Role of Neutrons. *Physical Review Letters* **111**(13), 131102 (2013). doi:10.1103/PhysRevLett.111.131102
- B. Paczyński, Gamma-ray bursters at cosmological distances. *Astrophys.J.Lett.* **308**, 43–46 (1986). doi:10.1086/184740
- A. Pe'er, Temporal Evolution of Thermal Emission from Relativistically Expanding Plasma. *Astrophys.J.* **682**, 463–473 (2008). doi:10.1086/588136
- A. Pe'er, "Photospheric Emission in Gamma-Ray Bursts", in *41st COSPAR Scientific Assembly*, COSPAR Meeting, vol. 41, 2016
- A. Pe'er, P. Mészáros, M.J. Rees, The Observable Effects of a Photospheric Component on GRB and XRF Prompt Emission Spectrum. *Astrophys.J.* **642**, 995–1003 (2006). doi:10.1086/501424
- A. Pe'er, B.-B. Zhang, F. Ryde, S. McGlynn, B. Zhang, R.D. Preece, C. Kouveliotou, The connection between thermal and non-thermal emission in gamma-ray bursts: general considerations and GRB 090902B as a case study. *M.N.R.A.S.* **420**, 468–482 (2012). doi:10.1111/j.1365-2966.2011.20052.x
- R. Preece, the Fermi collab., The First Pulse of the Extremely Bright GRB 130427A: A Test Lab for Synchrotron Shocks. *Science* **343**, 51–54 (2014). doi:10.1126/science.1242302
- S. Razzaque, P. Mészáros, E. Waxman, Neutrino tomography of gamma ray bursts and massive stellar collapses. *Phys. Rev.* **D68**, 083001 (2003)
- M.J. Rees, P. Mészáros, Unsteady outflow models for cosmological gamma-ray bursts. *Astrophys.J.Lett.* **430**, 93–96 (1994). doi:10.1086/187446
- M.J. Rees, P. Mészáros, Dissipative Photosphere Models of Gamma-Ray Bursts and X-Ray Flashes. *Astrophys.J.* **628**, 847–852 (2005). doi:10.1086/430818
- H. Riffert, A self-consistent shock solution for radiation-dominated flows. *Astrophys.J.* **327**, 760–771 (1988). doi:10.1086/166234
- E.M. Rossi, A.M. Beloborodov, M.J. Rees, Neutron-loaded outflows in gamma-ray bursts. *M.N.R.A.S.* **369**, 1797–1807 (2006). doi:10.1111/j.1365-2966.2006.10417.x
- M. Russo, C. Thompson, Hot Electromagnetic Outflows. I. Acceleration and Spectra. *Astrophys.J.* **767**, 142 (2013). doi:10.1088/0004-637X/767/2/142
- G.B. Rybicki, A.P. Lightman, *Radiative processes in astrophysics* 1979
- F. Ryde, The Cooling Behavior of Thermal Pulses in Gamma-Ray Bursts. *Astrophys.J.* **614**, 827–846 (2004). doi:10.1086/423782
- F. Ryde, A. Pe'er, T. Nymark, M. Axelsson, E. Moretti, C. Lundman, M. Battelino, E. Bissaldi, J. Chiang, M.S. Jackson, S. Larsson, F. Longo, S. McGlynn, N. Omodei, Observational evidence of dissipative photospheres in gamma-ray bursts. *M.N.R.A.S.* **415**, 3693–3705 (2011). doi:10.1111/j.1365-2966.2011.18985.x
- L. Sironi, A. Spitkovsky, Particle Acceleration in Relativistic Magnetized Collisionless Electron-Ion Shocks. *Astrophys.J.* **726**, 75 (2011). doi:10.1088/0004-637X/726/2/75
- C. Thompson, A Model of Gamma-Ray Bursts. *M.N.R.A.S.* **270**, 480 (1994)
- C. Thompson, R. Gill, Hot Electromagnetic Outflows. III. Displaced Fireball in a Strong Magnetic Field. *Astrophys.J.* **791**, 46 (2014). doi:10.1088/0004-637X/791/1/46
- C. Thompson, P. Mészáros, M.J. Rees, Thermalization in Relativistic Outflows and the Correlation between Spectral Hardness and Apparent Luminosity in Gamma-Ray Bursts. *Astrophys.J.* **666**, 1012–1023 (2007). doi:10.1086/518551
- N. Vlahakis, A. Königl, Relativistic Magnetohydrodynamics with Application to Gamma-Ray Burst Outflows. I. Theory and Semianalytic Trans-Alfvénic Solutions. *Astrophys.J.* **596**, 1080–1103 (2003). doi:10.1086/378226
- I. Vurm, A.M. Beloborodov, On the prospects of gamma-ray burst detection in the TeV band. *ArXiv e-prints* (2016a)
- I. Vurm, A.M. Beloborodov, Radiative Transfer Models for Gamma-Ray Bursts. *Astrophys.J.* **831**, 175 (2016b). doi:10.3847/0004-637X/831/2/175
- I. Vurm, A.M. Beloborodov, J. Poutanen, Gamma-Ray Bursts from Magnetized Collisionally Heated Jets. *Astrophys.J.* **738**, 77 (2011). doi:10.1088/0004-637X/738/1/77
- I. Vurm, R. Hascoët, A.M. Beloborodov, Pair-dominated GeV-Optical Flash in GRB

- 130427A. *Astrophys.J.Lett.* **789**, 37 (2014). doi:10.1088/2041-8205/789/2/L37
- I. Vurm, Y. Lyubarsky, T. Piran, On Thermalization in Gamma-Ray Burst Jets and the Peak Energies of Photospheric Spectra. *Astrophys.J.* **764**, 143 (2013). doi:10.1088/0004-637X/764/2/143
- E. Waxman, A. Loeb, TeV Neutrinos and GeV Photons from Shock Breakout in Supernovae. *Physical Review Letters* **87**(7), 071101 (2001). doi:10.1103/PhysRevLett.87.071101
- D.M. Wei, W.H. Gao, Are there cosmological evolution trends on gamma-ray burst features? *M.N.R.A.S.* **345**, 743–746 (2003). doi:10.1046/j.1365-8711.2003.06971.x
- D. Yonetoku, T. Murakami, T. Nakamura, R. Yamazaki, A.K. Inoue, K. Ioka, Gamma-Ray Burst Formation Rate Inferred from the Spectral Peak Energy-Peak Luminosity Relation. *Astrophys.J.* **609**, 935–951 (2004). doi:10.1086/421285
- D. Yonetoku, T. Murakami, S. Gunji, T. Mihara, K. Toma, T. Sakashita, Y. Morihara, T. Takahashi, N. Toukairin, H. Fujimoto, Y. Kodama, S. Kubo, IKAROS Demonstration Team, Detection of Gamma-Ray Polarization in Prompt Emission of GRB 100826A. *Astrophys.J.Lett.* **743**, 30 (2011). doi:10.1088/2041-8205/743/2/L30
- D. Yonetoku, T. Murakami, S. Gunji, T. Mihara, K. Toma, Y. Morihara, T. Takahashi, Y. Wakashima, H. Yonemochi, T. Sakashita, N. Toukairin, H. Fujimoto, Y. Kodama, Magnetic Structures in Gamma-Ray Burst Jets Probed by Gamma-Ray Polarization. *Astrophys.J.Lett.* **758**, 1 (2012). doi:10.1088/2041-8205/758/1/L1
- H.-F. Yu, H.J. van Eerten, J. Greiner, R. Sari, P. Narayana Bhat, A. von Kienlin, W.S. Paciesas, R.D. Preece, The sharpness of gamma-ray burst prompt emission spectra. *Astron.Astrophys.* **583**, 129 (2015). doi:10.1051/0004-6361/201527015